New Journal of Physics

The open access journal at the forefront of physics

PAPER

Classical and quantum dynamics of a trapped ion coupled to a charged nanowire

P N Fountas[1], M Poggio[2] and S Willitsch[1,3]

[1] Department of Chemistry, University of Basel, Klingelbergstrasse 80, 4056 Basel, Switzerland
[2] Department of Physics, Klingelbergstrasse 82, University of Basel, 4056 Basel, Switzerland
[3] Author to whom any correspondence should be addressed.

E-mail: stefan.willitsch@unibas.ch

CrossMark

OPEN ACCESS

Abstract

We study theoretically the mechanical drive of a trapped ultracold ion by a charged nanowire through their mutual Coulomb interaction. We characterize the perturbation of the trapping potential for the ion by the nanowire and discuss the parameters determining the dynamics of the ion under the action of the nanooscillator. We explore the classical dynamics as well as motional quantum states of the ion which can be generated and manipulated with the resonant drive of the nanowire and the effects of anharmonicities of the ion-trap potential on the system. Our modelling indicates that unusual quantum states of the ion motion can be generated with this approach and that sympathetic cooling and quantum entanglement can be realised when both subsystems operate in the quantum regime. The present ion-mechanical hybrid system might prove interesting as a new quantum device, for quantum sensing experiments, for spectroscopy and for mass spectrometry.

1. Introduction

Numerous efforts are currently aiming at the implementation of hybrid quantum systems in the quest for developing new devices for quantum technologies. The motivation for, e.g., a solid state-atomic interface emerges from the possibility to couple otherwise different platforms in order to combine the advantages of both. Recently, an impressive level of control over micro- and nanomechanical oscillators in the quantum regime has been achieved. The precise manipulation of the vibrational modes of mechanical oscillators, their control on the single-phonon level and their cooling to the quantum ground state have been demonstrated [1–4]. This progress has been enabled by cryogenic and optical cooling techniques. Furthermore, nanomechanical oscillators such as nanowires have appealing properties as ultrasensitive force sensors for nuclear magnetic resonance force microscopy [5], for the measurement of small friction forces [6] or for simultaneously detecting and imaging in-plane nanoscale force fields [7, 8]. Another asset of nanomechanical systems is their ability to interact with electromagnetic radiation over a wide range of the spectrum, which enables their interfacing with optical cavities [9], superconducting circuits [10] and quantum dots [11]. Apart from these appealing properties, a major drawback are their relatively poor coherence properties due to the coupling with their mechanical support and the environment, especially at room temperature.

Trapped ultracold ions or neutral atoms, by contrast, are systems which can exhibit excellent coherence properties. The coupling of ensembles of trapped ultracold atoms to nanomechanical oscillators has been explored in several theoretical studies [12–17] and has been realized experimentally recently [18, 19]. Trapped ultracold ions, on the other hand, can act themselves as mechanical oscillators through their tight confinement. Following ground state cooling of their motion in the trap, their internal and external degrees of freedom can be manipulated with high accuracy [20]. Zeeman [21], hyperfine [22] and optical [23] qubits have been implemented successfully in trapped ions. Controlled engineering of superpositions of spin and motional states of ion qubits with excellent coherence times has been achieved [24–26]. Parameters such as motional frequencies and dissipation can be changed on the fly. Moreover, by trapping multiple ions together one can form spatially well defined ordered structures called Coulomb crystals. In these systems, molecular ions can be
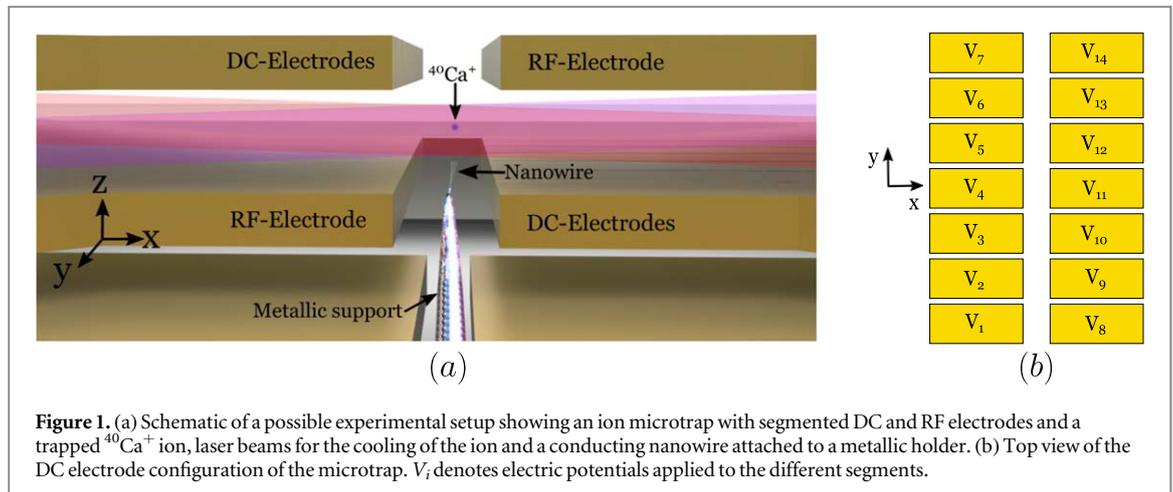
Figure 1. (a) Schematic of a possible experimental setup showing an ion microtrap with segmented DC and RF electrodes and a trapped ^{40}Ca$^+$ ion, laser beams for the cooling of the ion and a conducting nanowire attached to a metallic holder. (b) Top view of the DC electrode configuration of the microtrap. V_i denotes electric potentials applied to the different segments.

sympathetically cooled [27], and high-precision spectroscopic measurements [28] and controlled chemical reactions [29, 30] can be performed. Even a heat engine using a single trapped ion was recently demonstrated [31].

It appears appealing to combine all the aforementioned properties of nanomechanical and ionic systems. So far, there have been a few theoretical studies and proposals for hybrid systems consisting of trapped ions and nanooscillators [32–34]. In [32] it was proposed that an ion trap could be built from conductive nanowires or nanotubes, where one could realize the coupling of the nanoelectrodes with the motional modes of the ion. It was predicted that in this way the nanomechanical motion could be probed, the nanomechanical modes could be cooled, and entanglement between the fundamental modes of two nanoelectrodes could be realized via the ion. In general, such a system could be advantageous for the implementation of higher frequency ion traps with faster qubit gates for quantum computing. Similarly, in [33] it was demonstrated theoretically that the ion could be used as a probe for the quantum nature of mesoscopic oscillators and that the modes of the nanooscillator could be cooled down to its ground state via the ion. Conversely, in [34] it was argued that ion-based hybrid systems are in general not favourable for implementing a hybrid quantum system due the low coupling rates in comparison to the decoherence rates, and that trapped electrons may prove more advantageous for achieving higher coupling rates and for implementing faster gates.

In view of these varied and in parts contrasting predictions about the possibilities offered by ion-mechanical hybrid systems, we characterize here numerically a concrete experimental implementation of an ion-nanooscillator interface and explore its scientific prospects. Specifically, we study an ultracold ion coupled to a charged nanowire via their mutual electrostatic interaction. Using finite elements methods (FEM) calculations, the perturbation to the trapping potential of the ion by the nanowire is characterized, and suitable parameters are defined for an experimental implementation. In this context, the crucial challenge is to preserve the functionality of the ion trap in the presence of the nanowire. We present results of numerical calculations on the ion classical and quantum dynamics considering a classical mechanical drive of the nanooscillator. We also discuss the possibility of creation and read-out of Gaussian and non-Gaussian quantum states generated by this interaction. Finally, we address the prospects for sympathetic cooling and state exchange when both subsystems operate in the quantum regime.

2. Ion-nanooscillator hybrid system

A schematic of the specific experimental implementation under consideration is shown in figure 1. In the present study, we focus on ^{40}Ca$^+$ as a prototypical ion frequently used in ion-trap quantum technologies [23]. A single ^{40}Ca$^+$ ion is trapped in a miniaturized linear radiofrequency ion trap. The trap consists of two RF and two segmented DC electrodes (7 segments each) for the application of RF and DC voltages enabling a dynamic confinement of the ion. A cylindrical conductive nanowire attached to a metallic holder is positioned below the trap center. The diameter of the nanowire is assumed to be 200 nm and its tip is placed 50 μm away from the trap centre. In all calculations, the nanowire oscillates along the trap symmetry axis (y-axis). The tip-to-tip distance between the RF and DC electrodes is 400 μm creating a symmetric trapping potential for the ion exhibiting one axial and two degenerate radial oscillation frequencies.

In order to study the perturbation of the ion-trapping potential caused by the nanowire, FEM calculations were performed solving the Laplace equation using a three-dimensional electrostatic model [35]. For calculating the trap depth and the motional frequencies of the ion, the adiabatic approximation was used [36, 37]. Here, the
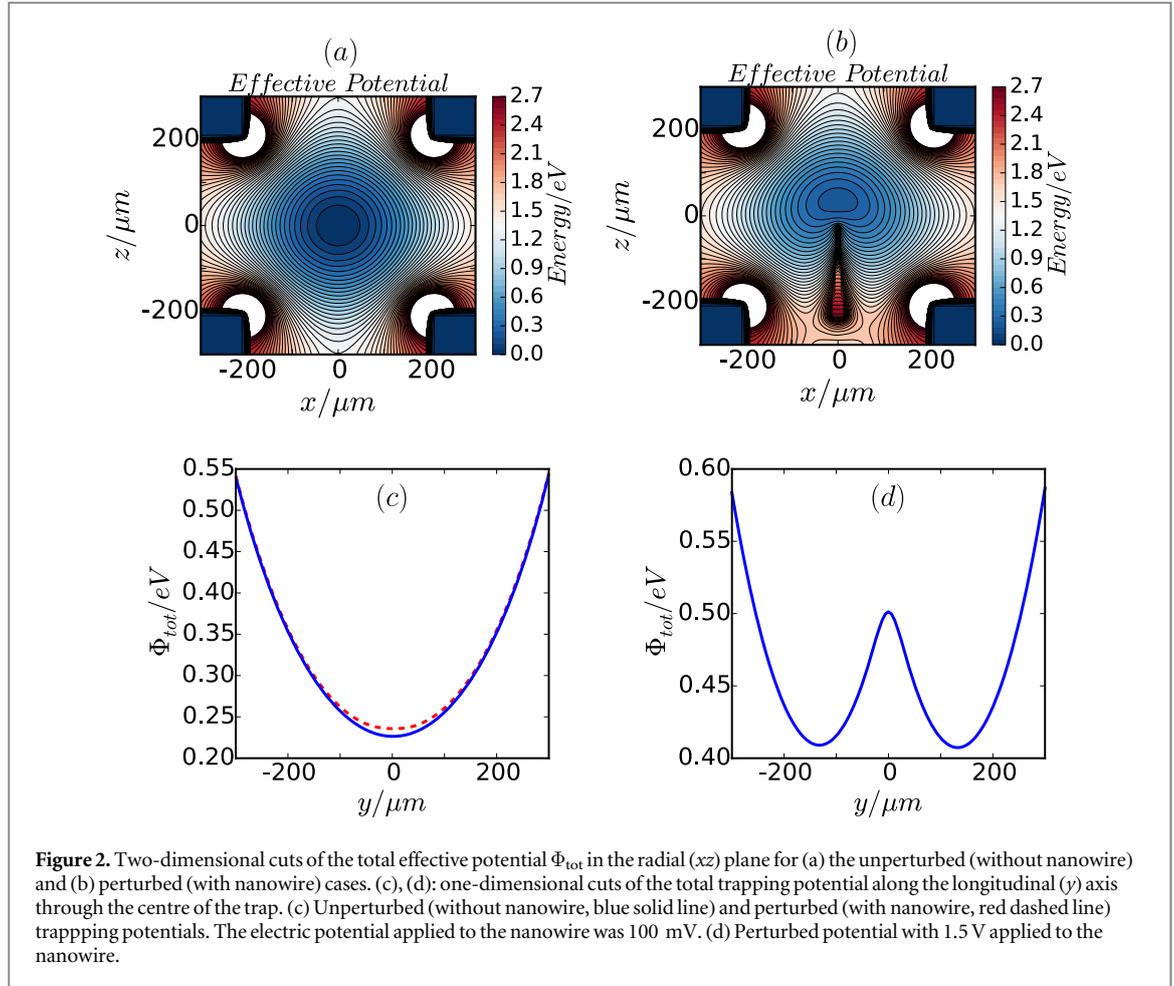
Figure 2. Two-dimensional cuts of the total effective potential Φ_{tot} in the radial (*xz*) plane for (a) the unperturbed (without nanowire) and (b) perturbed (with nanowire) cases. (c), (d): one-dimensional cuts of the total trapping potential along the longitudinal (*y*) axis through the centre of the trap. (c) Unperturbed (without nanowire, blue solid line) and perturbed (with nanowire, red dashed line) trappping potentials. The electric potential applied to the nanowire was 100 mV. (d) Perturbed potential with 1.5 V applied to the nanowire.

total effective trapping potential is expressed as the superposition of a time-independent RF pseudopotential and a static DC potential

$$\Phi_{tot} = \Phi_{RF} + \Phi_{dc} = \frac{V_{RF}^2 Q^2}{4 M \Omega_{RF}^2} ||\nabla \Phi_{RF}||^2 + Q \sum_i^n V_i \Phi_{dc,i}, \tag{1}$$

where M and Q are the mass and charge of the $^{40}Ca^+$ ion, V_{RF} and Ω_{RF} correspond to the RF amplitude and frequency, respectively, and Φ_{RF} stands for the RF potential basis function obtained from the calculations. The trap operating parameters were chosen such that the shape of the trapping potential is preserved under an electric potential of 100 mV applied to the nanowire, as can be seen in figure 2(c). This corresponds to the standard situation considered in the present work. The parameters used in the calculations were $V_{RF} = 150$ V, $\Omega_{RF}/2\pi = 35$ MHz and $V_i = \{V_1, V_2,\ldots,V_{14}\} = \{10, 8.43, 0, 0, 0, 8.43, 10, 10, 8.43, 0, 0, 0, 8.43, 10\}$ V. By calculating the Hessian matrix at the center of the trap, the secular frequencies for the oscillation of the ion along the three principal trap axes were determined as $\omega_x/2\pi = 1.85$ MHz, $\omega_y/2\pi = 600$ kHz and $\omega_z/2\pi = 1.87$ MHz. A two-dimensional cut of the total effective trapping potential in the radial (*xz*) plane is shown in figures 2(a) and (b) for the unperturbed (without nanowire) and perturbed (with nanowire) case, respectively.

By contrast, when applying 1.5 V to the nanowire, one can see in figure 2(b) a shift of the trapping minimum along the *z*-axis. One can clearly see from figure 2(b) that the trap is preserved under these conditions. Along the longitudinal trap axis (*y*), a double-well potential is formed under these conditions as can be seen in figure 2(d). The ion will be trapped in one of the potential wells at a new equilibrium position 130 μm away from the initial one with a modified oscillation frequency. One can tune the height of the barrier between the two wells by increasing or decreasing the voltage of the nanowire or its distance from the trap center, while maintaining a stable three-dimensional trap for the ion. We observe from figure 2(d) that at 1.5 V the height of the barrier is around 100 meV, which is enough for a single ion to be confined in one of the two wells. Note that our FEM simulations indicate that no significant shift of the trap minimum or deformation of the trap potential occurs when the nanowire is grounded.

The RF field of the trap is not expected to significantly affect the motion of the nanowire due to the large difference of the RF frequency of the trap Ω_{RF} and the oscillation frequency of the nanowire ω_{nw}. Moreover, RF pickup by the nanowire can be suppressed by a filter capacitor. A bias voltage on the nanowire may shift the ion

from the symmetry axis of the trap causing excess micromotion [38]. This can be compensated by appropriate potentials applied to the DC electrodes. Note that the calculations presented in the following are only considering the dynamics of the ion along the symmetry axis of the trap which are unaffected by small radial displacements.

If the nanowire is not mechanically driven, it still thermally oscillates with an amplitude on the order of 1 nm at room temperature. We find numerically that with typical potentials of 100 mV applied, the thermal motion is too small in order to induce any significant dynamics on the ion on the timescales considered here. Note also that when the nanowire is grounded, the leading terms of its interaction with the ion vanish (see equation (3) below) and it merely acts as an additional grounded electrode.
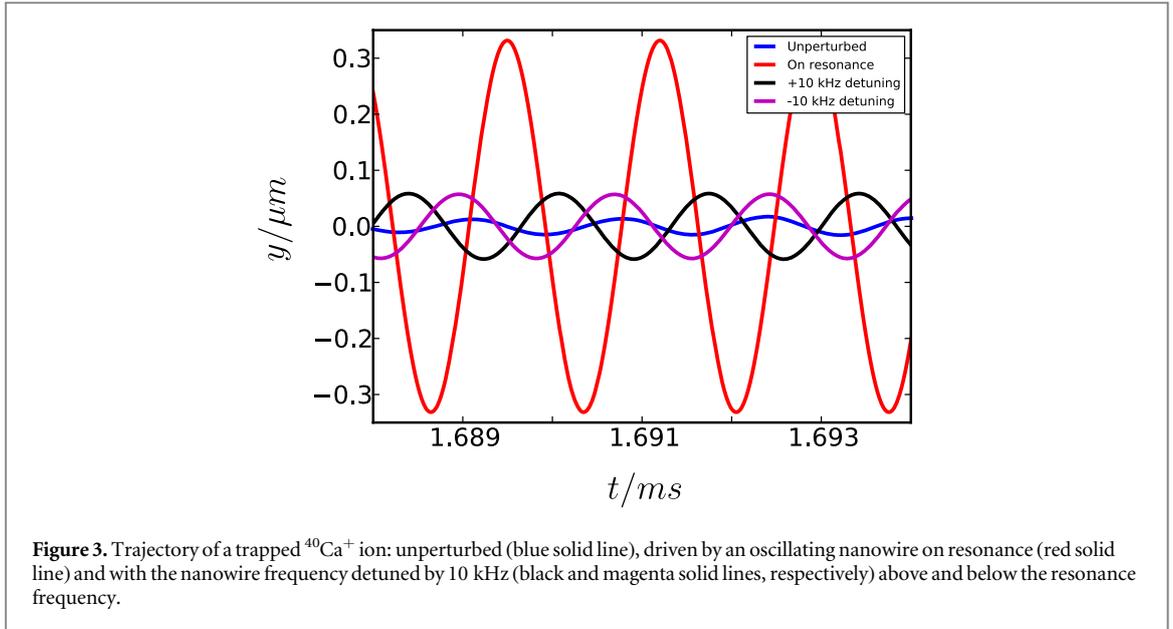
3. Computational model

We now turn to studying resonant mechanical coupling of a trapped $^{40}Ca^+$ ion with a charged nanowire interacting via their electrostatic repulsion. The axial motional frequency of the ion in the trap is assumed to be 600 kHz, which will also be the frequency of one of the first two fundamental modes of the nanowire. The benefit of driving the nanowire along the symmetry axis of the trap is the easy matching with the ion frequency by tuning the voltages applied to the DC electrodes of the trap. The nanowire is assumed to be at room temperature. From a Maxwell–Boltzmann distribution , we calculate that the nanowire at 300 K will have around 15 million phonons. We approximate the effect of the nanowire as the one of a classical electric field generated by a spherically charged particle at its tip acting on the motion of the ion corresponding to the leading term in the electrostatic interaction between the two charge distributions. Thus, the interaction potential in three dimensions reads

$$U_c = \frac{k_c Q_1 Q_2}{\sqrt{x^2 + (y - Y(t))^2 + (z + d)^2}}, \qquad (2)$$

where k_c is the Coulomb constant, Q_1 and Q_2 are the charges of the ion and the nanowire, respectively, x, y, z are the coordinates of the ion, d is the relative distance between the ion and the nanowire, and $Y(t) = A \cos(\omega_{nw} t)$ describes the driving field generated by the nanowire with a specific amplitude A and frequency of oscillation ω_{nw}. The point of origin of the coordinate system is taken to be at the equilibrium position of the ion.

4. Classical dynamics

Before we turn to quantum dynamics, we briefly consider the classical motion of the ion under the action of the nanowire modeled using molecular dynamics (MD) simulations [27]. The force model used includes the force field of the trap, a friction force that describes the ion cooling through its interaction with a laser field and a coupling force that describes the interaction of the ion with the charged nanowire as described above [27]. Heating of the ion caused by collisions with background gas or by experimental imperfections are included as random momentum kicks with specific magnitude. The Newtonian equations of motion are solved numerically using the Leapfrog integrator implemented in the ProtoMol MD simulations software [39]. The nanowire is driven along the y-axis resonant with the axial frequency of the ion at $\omega_y/2\pi = 600$ kHz with an amplitude of oscillation of 100 nm. The charge of the biased nanowire used for both the classical and quantum calculations is $Q = 1.6 \times 10^{-18}$ C. After setting initial positions and velocities of the $^{40}Ca^+$ ion, the MD simulations are initiated with the trapping and friction force fields. The initial temperature of the ion is 40 μK and the nanowire drive is operative during the whole simulation time. Figure 3 shows a snapshot of the MD simulations representing the ion axial trajectory for the resonant case as well as with the nanooscillator frequency detuned 10 kHz above and below the resonance frequency. In the simulation, the drive of the nanowire is continuous while Doppler laser cooling of the ion is maintained. At the time shown, the system has reached a steady state. The blue line represents the unperturbed motion of the ion, the red line represents the ion motion after the nanowire resonant drive and the other lines show the ion motion when the nanowire frequency is detuned by 10 kHz. The unperturbed motion of the ion corresponds to an oscillation with an amplitude of 10 nm. As expected, a resonant drive of the ion by the nanowire couples energy into the ion motion which reaches amplitudes up to 300 nm in the present case. The efficiency of the coupling, however, reduces quickly with increasing mismatch between the ion and nanowire oscillation frequencies.

Figure 3. Trajectory of a trapped ^{40}Ca$^+$ ion: unperturbed (blue solid line), driven by an oscillating nanowire on resonance (red solid line) and with the nanowire frequency detuned by 10 kHz (black and magenta solid lines, respectively) above and below the resonance frequency.

5. Quantum dynamics

To model the quantum dynamics of the ion under the action of the nanowire, the ion-nanowire interaction potential was expanded in a Taylor series, as also discussed in [12], up to second order for small excursions of the ion around its equilibrium position:

$$U_c = \frac{\epsilon}{d} - \frac{\epsilon}{d^2} z - \frac{\epsilon}{2d^3} x^2 - \frac{\epsilon}{2d^3} y^2 + \frac{\epsilon}{d^3} z^2 + \frac{\epsilon A}{d^3} y \cos(\omega_{\mathrm{nw}} t) - \frac{\epsilon A^2}{2d^3} \cos^2(\omega_{\mathrm{nw}} t), \tag{3}$$

where $\epsilon = k_c Q_1 Q_2$. The first and last terms are energy offsets which do not affect the dynamics of the system. The degrees of freedom along the y-axis are decoupled from x and z so that the driven dynamics can be described in one dimension. The Hamiltonian is quantized by replacing the position coordinates with the position operators in the Fock basis. The total Hamiltonian including the trapping potential is written as

$$\hat{\mathcal{H}}_{\mathrm{tot}} = \hbar\omega(\hat{a}^\dagger \hat{a} + \frac{1}{2}) - \frac{\epsilon}{2d^3} \frac{\hbar}{2m\omega} (\hat{a}^\dagger + \hat{a})^2 + \frac{\epsilon A}{d^3} \sqrt{\frac{\hbar}{2m\omega}} (\hat{a}^\dagger + \hat{a}) \cos(\omega_{\mathrm{nw}} t), \tag{4}$$

where $\hat{y} = (\hbar/2 m\omega)^{1/2} (\hat{a}^\dagger + \hat{a})$ and the factor $(\hbar/2m\omega)^{1/2}$ corresponds to the zero point fluctuations. $\omega \equiv \omega_y$ and $\hat{a}$, $\hat{a}^\dagger$ are the annihilation and creation operators of the motional degrees of freedom of the ion in the harmonic trap.

Re-expressing this Hamiltonian in frequency units we get

$$\hat{\mathcal{H}}_{\mathrm{tot}} = \omega\left(\hat{a}^\dagger \hat{a} + \frac{1}{2}\right) - s(\hat{a}^\dagger + \hat{a})^2 + g(\hat{a}^\dagger + \hat{a}) \cos(\omega_{\mathrm{nw}} t), \tag{5}$$

where $s = \epsilon/(4m\omega d^3)$ and $g = [\epsilon A/(\hbar d^3)][\hbar/(2m\omega)]^{1/2}$. The first term is the energy of a quantum harmonic oscillator which describes the unperturbed motion of the ion in the trap. The other two terms are the contributions of the effect of the nanowire to the motion of the ion. The second term, which is quadratic in the sum of the ladder operators, gives a shift to the ion vibrational levels and also introduces squeezing. The last term incorporates the coupling to the driving field and also introduces displacement of the ion.
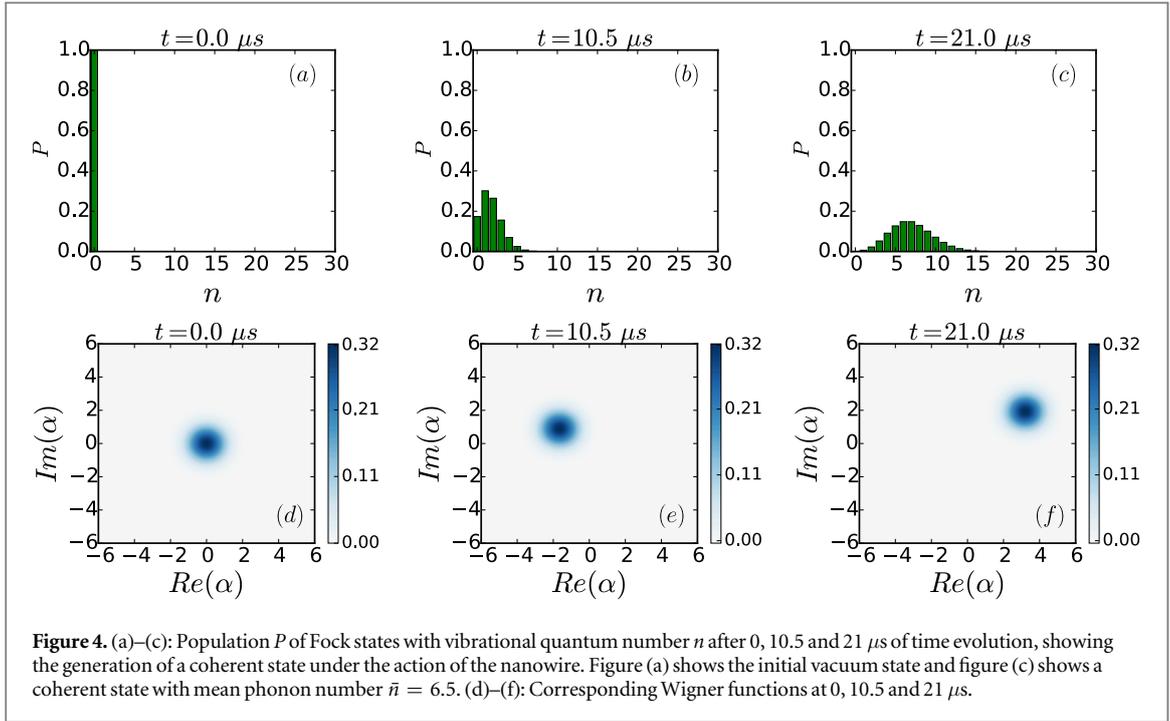
The corresponding Schrödinger equation was solved in the interaction picture. All quantum-dynamics calculations were performed using the quantum toolbox in python (QuTip) [40, 41]. Decoherence effects were included numerically by solving the Lindblad master equation

$$\frac{d\hat{\rho}}{dt} = -\frac{i}{\hbar} [\hat{\mathcal{H}}_{\mathrm{tot}}, \hat{\rho}] + \hat{\mathcal{L}}\hat{\rho}, \tag{6}$$

with

$$\hat{\mathcal{L}}[\hat{C}]\hat{\rho} = \sum_{i=1}^{N^2-1} \gamma_i\left(\hat{C}_i \hat{\rho} \hat{C}_i^\dagger - \frac{1}{2}\{\hat{C}_i^\dagger \hat{C}_i, \hat{\rho}\}\right), \tag{7}$$

where $\hat{\rho}$ is the density matrix of the system and $\hat{\mathcal{L}}$ is the Lindblad superoperator which describes the decoherence of the corresponding degrees of freedom [42].

Figure 4. (a)–(c): Population P of Fock states with vibrational quantum number n after 0, 10.5 and 21 μs of time evolution, showing the generation of a coherent state under the action of the nanowire. Figure (a) shows the initial vacuum state and figure (c) shows a coherent state with mean phonon number $\bar{n} = 6.5$. (d)–(f): Corresponding Wigner functions at 0, 10.5 and 21 μs.

The decoherence rate γ of the ion was assumed to be on the order of 4–10 Hz. We also performed various calculations by assuming different ion decoherence rates from 20 to 60 Hz, which are values that are experimentally reasonable. We found that decoherence rates of this magnitude are small compared to the stronger driven dynamics of the system and barely have any effect on the present results. During the entire period covered in the calculations, we assumed that the laser cooling of the ion is switched off and a constant drive is applied to the nanowire with a specific frequency and amplitude of oscillation.

As initial conditions in our calculations, we assumed a $^{40}Ca^+$ ion cooled to the motional ground state of a trap with $\omega_y / 2\pi = 600$ kHz axial frequency. The nanowire was fixed at a position 50 μm away from the ion along the z-axis and driven at 100 nm amplitude at $\omega_{nw} / 2\pi = 600$ kHz. A voltage of 100 mV was applied. Figure 4 shows snapshots of the dynamics within the first 30 vibrational levels of the trap. Figures 4(a)–(c) show the populations and figures 4(d)–(f) show the Wigner functions at 0, 10.5 and 21 μs into the dynamics. The Wigner function (a phase-space quasi-probability distribution) is defined for an arbitrary density operator $\hat{\rho}$ as [43]

$$W(q, p) = \frac{1}{2\pi\hbar} \int_{-\infty}^{\infty} \langle q + \tfrac{1}{2}x| \hat{\rho} | q - \tfrac{1}{2}x \rangle e^{-ipx/\hbar} dx. \tag{8}$$
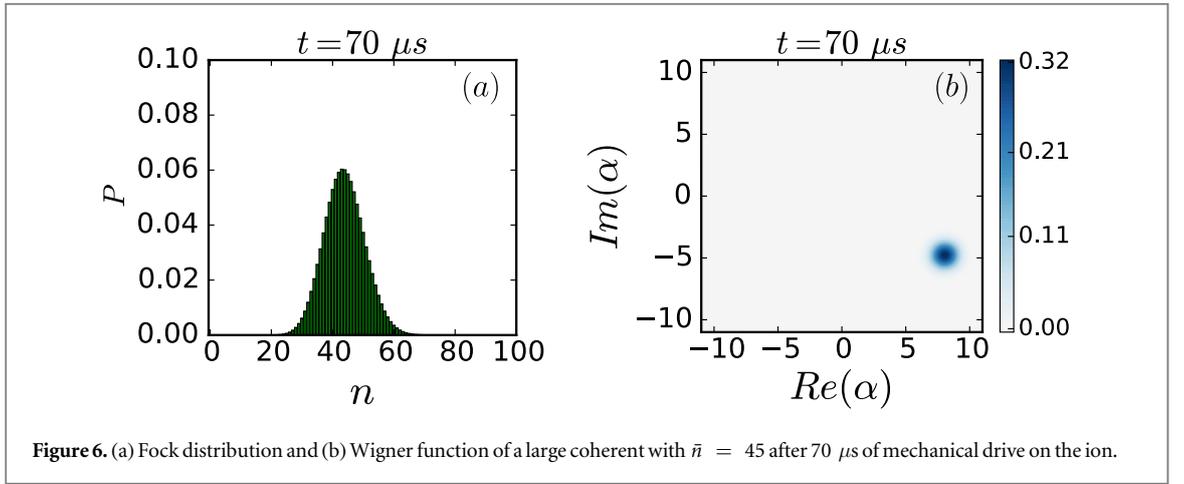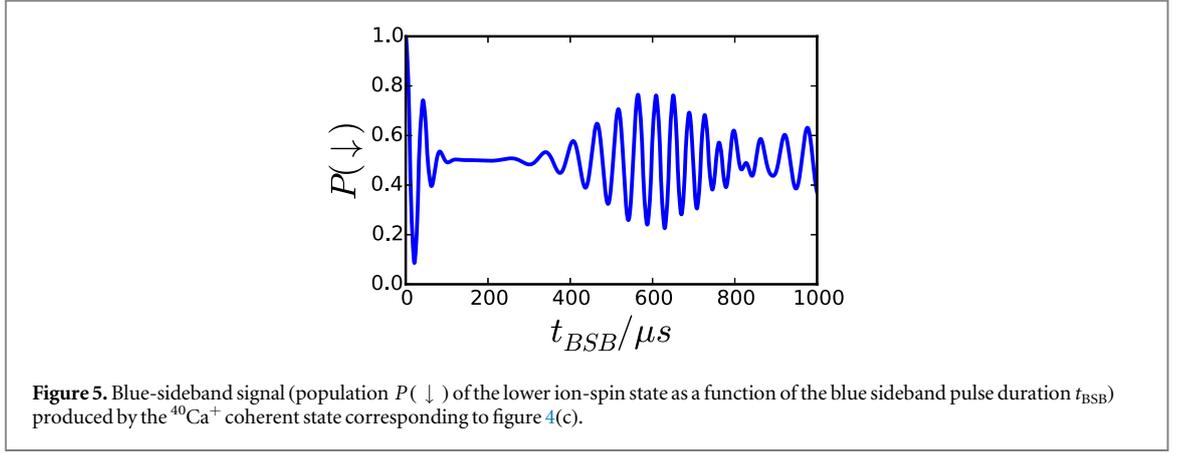
Essentially, figure 4 shows the creation of a coherent state of the ion motion under the action of the nanowire. We interpret this result as the mapping of the nanowire's coherent motion onto the ion motional degrees of freedom.

Experimentally, the readout of the state of the ion can be performed with well established techniques as reported in, e.g., [24, 25]. A two-state pseudo-spin system can be realized by addressing the $(4s)\ ^2S_{1/2} \rightarrow (3d)\ ^2D_{5/2}$ quadrupole transition in Ca^+ with a 729 nm laser. The blue-sideband Hamiltonian for this transition reads [20]

$$\hat{H}_{bsb} = \frac{\hbar}{2} \Omega_0 \eta (\hat{a}^\dagger \hat{\sigma}_+ + \hat{a}\hat{\sigma}_-), \tag{9}$$

where Ω_0 is the Rabi frequency, η is the Lamb-Dicke parameter, and $\hat{\sigma}_+$ and $\hat{\sigma}_-$ are the spin ladder operators. This Hamiltonian couples the motional and spin degrees of freedom of the ion. The experimental signal, i.e. the population in the lower spin state $P(\downarrow)$ produced by this interaction is shown in figure 5 where we assume a Rabi frequency of $\Omega_0 / 2\pi = 70$ kHz for the blue sideband oscillation.

This way of generating a coherent state is similar to the one reported in [24], where an oscillating electric field was applied to one of the trap electrodes. In comparison, the case considered here of a static field applied to an oscillating nano-resonator may offer some advantages. For example, one can tune the dynamics of the state generation on-the-fly by varying the position or voltage of the nanowire. Another advantage of this scheme is that the generation of the ion quantum states is independent of laser or magnetic field fluctuations, since the nanowire interacts directly with the ion motional degrees of freedom, in contrast to the generation of coherent states with a laser field where the ion motional and spin degrees of freedom are coupled. A disadvantage of the

Figure 5. Blue-sideband signal (population $P(\downarrow)$ of the lower ion-spin state as a function of the blue sideband pulse duration t_{BSB}) produced by the $^{40}Ca^+$ coherent state corresponding to figure 4(c).

Figure 6. (a) Fock distribution and (b) Wigner function of a large coherent with $\bar{n} = 45$ after 70 μs of mechanical drive on the ion.

optical field is that it interacts with an electric dipole or quadrupole moment of the atomic ion and the oscillator states prepared in this way are typically limited to excitations of <20 quanta. The charged nanowire, on the other hand, acts directly on the electric monopole and therefore large-amplitude coherent states can be created without the need of electronics for fast switching trapping potentials [44] as seen in figure 6. This figure shows the Fock distribution and Wigner function of a large coherent state with $\bar{n} = 45$ after 70 μs of driving dynamics.
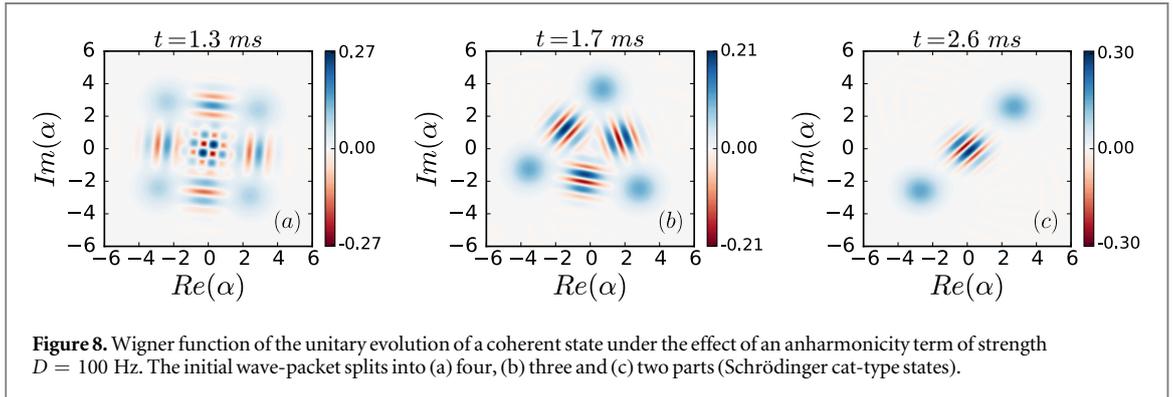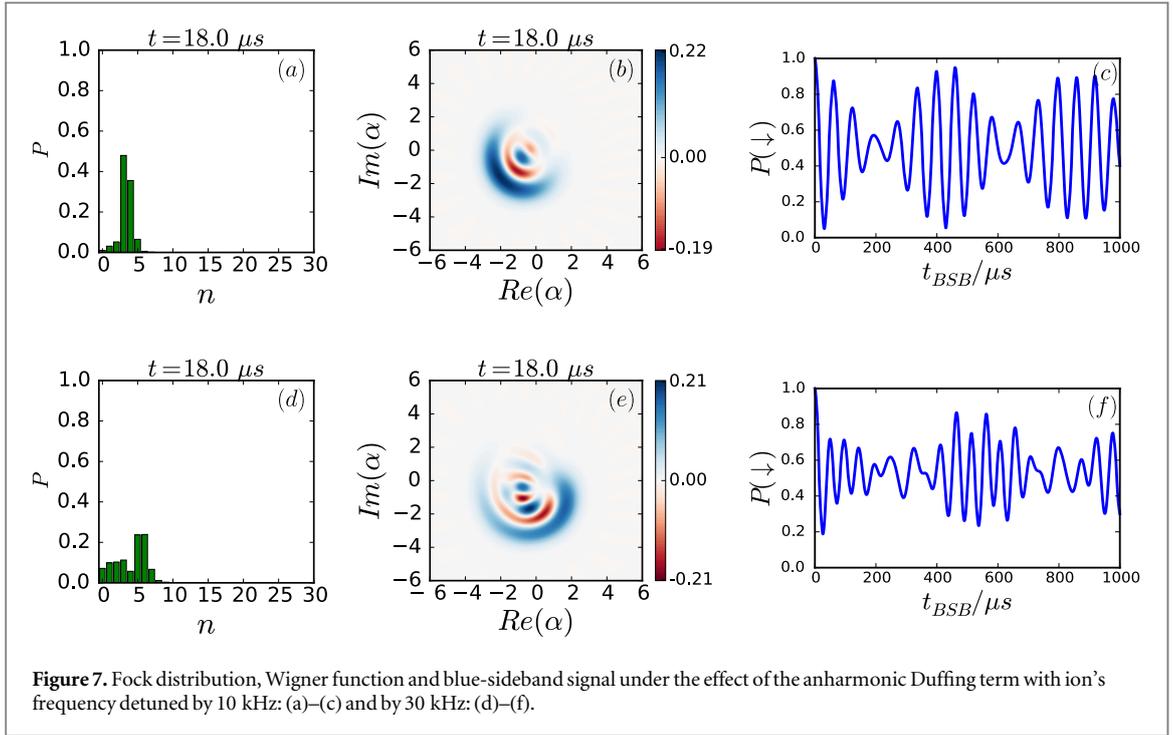
In addition to the creation of coherent states, it is of interest to investigate the possibility of creating non-Gaussian states with the same drive. This can be achieved by additionally employing anharmonicities in the trapping potential. The Hamiltonian of equation (5) can be augmented with the anharmonic contribution:

$$\hat{\mathcal{H}}_{tot} = \omega\left(\hat{a}^\dagger\hat{a} + \frac{1}{2}\right) - s(\hat{a}^\dagger + \hat{a})^2 + g(\hat{a}^\dagger + \hat{a})\cos(\omega_{nw}t) + D(\hat{a}^\dagger + \hat{a})^4, \tag{10}$$

where D is the strength of the anharmonic (Duffing) term of the axial trap potential.

Such anharmonicities may arise from different sources in an ion trap, like patch potentials or geometric asymmetries of the electrodes close to the trapping region. Additionally, one can engineer anharmonicities and consequently the Duffing term in equation (10) by varying the voltages on the DC electrodes [45]. As an example, figures 7(a) and (d) show the populations and figures 7(b) and (e) the Wigner functions of non-Gaussian states generated with a detuning of 10 and 30 kHz of the nanowire to the ion motional frequency, respectively, and introducing an anharmonicity of $D = 8$ kHz that corresponds to a DC voltage configuration $V_i = \{V_1, V_2,\ldots,V_{14}\} = \{10, 9, 0, 1.58, 0, 9, 10, 10, 9, 0, 1.58, 0, 9, 10\}$ V. The first row of figure 7, i.e. 7(a)–(c), corresponds to the $^{40}Ca^+$ ion at 10 kHz axial detuning and the second row, i.e. 7(d)–(f), corresponds to the $^{40}Ca^+$ ion at 30 kHz detuning. All of these figures show snapshots of the dynamics at the same time step of 18 μs. Figures 7(c) and (f) show the corresponding blue-sideband signal of the non-Gaussian states. Under these conditions, we see that the initial vacuum state is diffused and the appearance of the negative regions in the Wigner function is a signature of genuine quantum states, as compared to the quasi-classical Gaussian ones of figure 4.

Alternatively, one can create a coherent state in a region of the potential where anharmonicities exist. In the calculations, we assume a strength of the anharmonicity term of $D = 100$ Hz. After the voltage of the nanowire

Figure 7. Fock distribution, Wigner function and blue-sideband signal under the effect of the anharmonic Duffing term with ion's frequency detuned by 10 kHz: (a)–(c) and by 30 kHz: (d)–(f).

Figure 8. Wigner function of the unitary evolution of a coherent state under the effect of an anharmonicity term of strength $D = 100$ Hz. The initial wave-packet splits into (a) four, (b) three and (c) two parts (Schrödinger cat-type states).

has been switched off, this coherent state evolves under the effect of the anharmonicites and dynamically transforms into different quantum states for different time steps of its evolution as can be seen in figure 8. We clearly see that the initial Gaussian wave-packet splits into Schrödinger cat-type states with four, three and two parts [46] at 1.3, 1.7 and 2.6 ms under this unitary evolution, creating interference pattern between its different Gaussian parts. However, the Fock-state distribution of all these three quantum states is the same as with the initial coherent state as in figure 4(c). This effect makes these states experimentally undetectable with a simple blue sideband pulse which is directly connected to the Fock-state distribution but not the phases of the initial coherent state. To detect these states, more sophisticated techniques like quantum state tomography have to be applied for the direct reconstruction of the density matrix of the system [23].

Concluding the dynamics of the system with a nanowire at room temperature, we investigated the ion phonon dynamics under the action of the oscillating nanowire detuned from resonance for a continuous drive and taking into account the nanoresonator dissipation. In figures 9 (a)–(c), the mean phonon number for (a) a resonant drive, (b) a detuning of 10 kHz between the ion and the nanowire frequencies under a continuous drive, and (c) a detuning of 10 kHz and including the attenuation of the nanowire. The attenuation of the nanowire is included as an exponential decay of its amplitude with a rate of 10 kHz. With this detuning, not more than 20 phonons of the ion can be excited, and a good description is achieved by including the first 30 vibrational levels in the Hilbert space. On resonance, the excitation is so strong that the nanowire excites more and more phonons. For the off-resonant case, we observe that the ion experiences excitation and de-excitation, which is due to alternating in-phase and out-of-phase motion between the ion and the nanowire. This shows that even at room temperature, one can use the ion as a probe for the nanowire's motion and experimentally study phase shifts and dissipation mechanisms of mesoscopic systems.
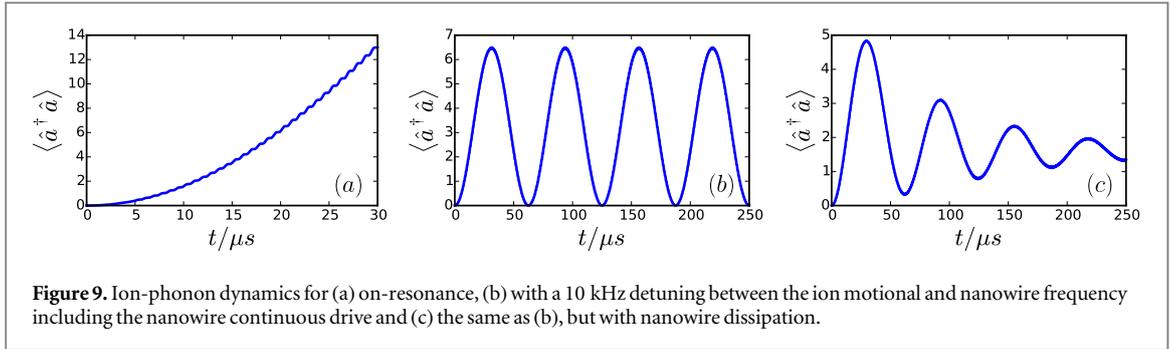
Figure 9. Ion-phonon dynamics for (a) on-resonance, (b) with a 10 kHz detuning between the ion motional and nanowire frequency including the nanowire continuous drive and (c) the same as (b), but with nanowire dissipation.

Finally, we consider the situation in which both the ion and the nanoscillator operate in the quantum regime, as would be the case in a cryogenic experiment in which the nanowire is cooled close to the quantum-mechanical ground state of one or several of its modes. At cryogenic temperatures, we can describe the nanowire's motion with ladder operators in the Fock space and now the fully quantized Hamiltonian for the coupling between the nanowire and the ultracold ion reads

$$\hat{\mathcal{H}}_{\mathrm{coupling}} = g(\hat{a}^\dagger + \hat{a})(\hat{b}^\dagger + b),$$
$$\mathrm{with}\ g = \frac{\hbar\epsilon}{2d^3}\frac{1}{\sqrt{mM}}\frac{1}{\sqrt{\omega\,\omega_{\mathrm{nw}}}}. \tag{11}$$

Here, g is the coupling strength, $\epsilon = k_c Q_1 Q_2$ and d is the relative distance between the tip of the nanowire and the ion. m, ω and M, ω_{nw} are the mass and the oscillation frequency of the ion and the nanowire, respectively. We see that the coupling strength is inversely proportional to the product of the masses of those two systems. Conventional metallic nanowires exhibit very high masses ($M \approx 10^{-14}$ kg) compared to single ions which renders the coupling between the two systems very small. This can be mitigated by using carbon nanotubes instead ($M \approx 10^{-20} - 10^{-23}$ kg), which are very good conductors in specific configurations [47, 48]. The second dominant limitation towards achieving strong coupling is the mechanical decoherence rate of the nanowire caused by its coupling to the bath. A nanowire with a mechanical Q-factor of 300 000 and an oscillation frequency of $\omega_{\mathrm{nw}}/2\pi = 600$ kHz has about 10^5 motional quanta of thermal excitation when it is coupled to a bath with a temperature of 4.2 K. The thermal decoherence rate of the nanowire is given by $\gamma_{\mathrm{nw}} N_{\mathrm{nw}} = k_b T/\hbar Q_{\mathrm{nw}}$ where k_B is the Boltzmann constant and T is the bath temperature. The mechanical quality factor is given by $Q_{\mathrm{nw}} = \omega_{\mathrm{nw}}/\gamma_{\mathrm{nw}}$ where γ_{nw} is the mechanical decoherence rate of the nanowire due to its coupling with the bath. This corresponds to a thermal decoherence rate of around 300 kHz for the nanowire. With these assumptions, the Lindblad master equation of the coupled system
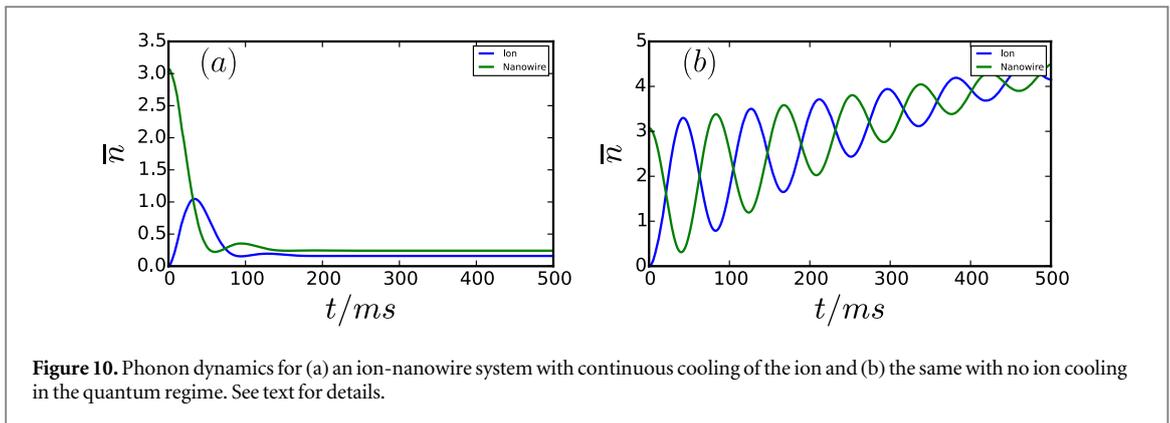
$$\frac{\mathrm{d}\hat{\rho}}{\mathrm{d}t} = -\frac{\mathrm{i}}{\hbar}\,[\hat{\mathcal{H}}_{\mathrm{eff}},\,\hat{\rho}] + \gamma_{\mathrm{ion}}^{\mathrm{heating}}\,\hat{\mathcal{L}}[\hat{a}^\dagger]\hat{\rho} + \gamma_{\mathrm{ion}}^{\mathrm{cooling}}\,\hat{\mathcal{L}}[\hat{a}]\hat{\rho}$$
$$+ \gamma_{\mathrm{nw}}(N_{\mathrm{nw}} + 1)\,\hat{\mathcal{L}}[\hat{b}]\hat{\rho} + \gamma_{\mathrm{nw}}N_{\mathrm{nw}}\,\hat{\mathcal{L}}[\hat{b}^\dagger]\hat{\rho} \tag{12}$$

was solved numerically. Here, $\gamma_{\mathrm{ion}}^{\mathrm{heating}}$ is the heating rate of the ion in a trap, $\gamma_{\mathrm{ion}}^{\mathrm{cooling}}$ is the cooling rate of the ion from the interaction with the cooling laser. The total effective Hamiltonian of the system is

$$\hat{\mathcal{H}}_{\mathrm{eff}} = \hbar\omega\left(\hat{a}^\dagger\hat{a} + \frac{1}{2}\right) + \hbar\omega_{\mathrm{nw}}(\hat{b}^\dagger\hat{b} + \frac{1}{2}) + g(\hat{a}^\dagger + \hat{a})(\hat{b}^\dagger + \hat{b}). \tag{13}$$

Choosing the parameters $m = 6.6 \times 10^{-26}$ kg, a conservative value of $M = 6.6 \times 10^{-20}$ kg, $\omega/2\pi = \omega_{\mathrm{nw}}/2\pi = 600$ kHz, $d = 50\,\mu$m and a voltage of $V_{\mathrm{nw}} = 100$ mV on the nanowire, the coupling strength between the ion and the nanowire is $g/2\pi = 37$ Hz. The mass ratio between the ion and the nanowire should be at most $m/M = 10^{-6}$ for a coupling between the two systems to be feasible at this magnitude. The frequency shift of the nanowire caused by the ion is negligible and was omitted from the calculations. The frequency shift of the ion caused by the nanowire at the chosen parameters is 6 kHz. Thus, a 6 kHz detuning was assumed for the ion in order to match the frequencies of the two oscillators in order to study the resonant case. An intriguing possibility in this regime is the sympathetic cooling of the nanowire by the ion. The cooperativity parameter, given by $C = 4g^2/\gamma_{\mathrm{ion}}\gamma_{\mathrm{nw}}$, should be $C > 1$ in order for sympathetic cooling of the nanowire to be feasible [13]. For a bath temperature of $T = 4.2$ K which can be achieved with standard cryostats and $g/2\pi = 37$ Hz, $\gamma_{\mathrm{ion}}/2\pi = 4$ Hz, $\gamma_{\mathrm{nw}}/2\pi = 300$ kHz, one calculates $C = 0.0047$. Consequently, at 4.2 K bath temperature and such a big mass mismatch, the coupling is very weak, and neither coherent dynamics nor sympathetic cooling of the nanowire should be observable under these conditions. Coherent dynamics can only be observed at much lower temperatures. Indeed, we found that when the temperature is above 500 μK, the nanowire essentially behaves like a classical object vis-a-vis the ion.

Figure 10. Phonon dynamics for (a) an ion-nanowire system with continuous cooling of the ion and (b) the same with no ion cooling in the quantum regime. See text for details.

This behaviour changes at very low temperatures of the nanowire. Figures 10(a) and (b) show the coherent phonon dynamics of the hybrid system with and without continuous sideband cooling of the ion, respectively, at a nanowire bath temperature of $T = 100\,\mu$K and all other parameters kept the same as before. It should be noted that such a bath temperature is close to the current state of the art [49], but will be extremely challenging to achieve as it is about two orders of magnitude lower than what can be achieved in commercially available dilution refrigerators.

It can be seen from figure 10(a) that the nanowire is sympathetically cooled from a single ultracold ^{40}Ca$^+$ within the first 60 ms with a cooling rate of 0.05 quanta ms^{-1}. Figure 10(b) shows the energy swap between the nanowire and the ion. In the absence of an ion cooling mechanism, the coherent phonon dynamics are more clearly manifested. Eventually both systems equilibrate with the bath reaching an average of approximately 4 phonons each.

Moreover, every time that the system undergoes an energy swap as shown in figure 10(b), there is a transfer of the quantum state between the ion and the nanowire as is shown in figure 11. Figures 11(a) and (b) show the initial Wigner functions of an ultracold ion and a nanowire in the zeroth and fourth Fock states, respectively. Figures 11(c) and (d) show the relevant Wigner function after 41 ms of interaction time, after which one cycle of energy swap has occurred according to figure 10(b). It can be seen that the states of the ion and the nanowire have essentially been exchanged. The different intensities of the Wigner functions and the slightly larger spread of the vacuum state of the nanowire compared to the initial states are attributed to the thermal decoherence of the hybrid system. We have seen the same type of behaviour for various initial quantum states for both of the systems including Fock, coherent, squeezed and thermal states. Therefore, this interaction allows us to create a specific quantum state in one of these two systems and read it out from the other. This might be an interesting approach for studying decoherence mechanisms or creating quantum gates between solid-state and ionic systems, opening up possibilities for new quantum devices.

6. Summary and conclusions

We have studied numerically the classical and quantum dynamics of a trapped ion under the action of an oscillating charged nanowire in the context of a setup which is realizable with current technology. We have explored possibilities of creating Gaussian and non-Gaussian motional states of the ion by a classical mechanical drive of the nanowire held at room temperature. We showed the creation of coherent states of the ion motion by mapping the coherent motion of the nanowire indicating that an ultracold ion could be used as a probe for a nanomechanical system. Non-Gaussian states were found to emerge dynamically under the influence of additional trap anharmonicities. Within a full quantum treatment of both subsystems, our calculations suggest the possibility of sympathetic cooling of a light nanowire such as a carbon nanotube by an ultracold ion if the nanowire can be precooled to the quantum regime. Also, it seems possible to create specific motional quantum states of the ion and map them onto the nanowire, and vice versa. This might be interesting in the context of quantum sensing experiments, for instance if a squeezed state is generated in one system and is then mapped to the other. However, we generally do not expect a strong back-action from a single ion onto the nanowire, due to their large mass difference in line with the predictions of [34]. Nonetheless, the present study suggests that even when the nanooscillator is operating in the classical regime, it can serve as a useful tool for engineering motional quantum states of the ion which may be challenging to generate with other means. The present system may prove fruitful for various applications, e.g. as a new way to shape ion-trapping potentials, as a probe of decoherence processes of quantum and macroscopic bodies, in mass spectrometry and in quantum sensing.
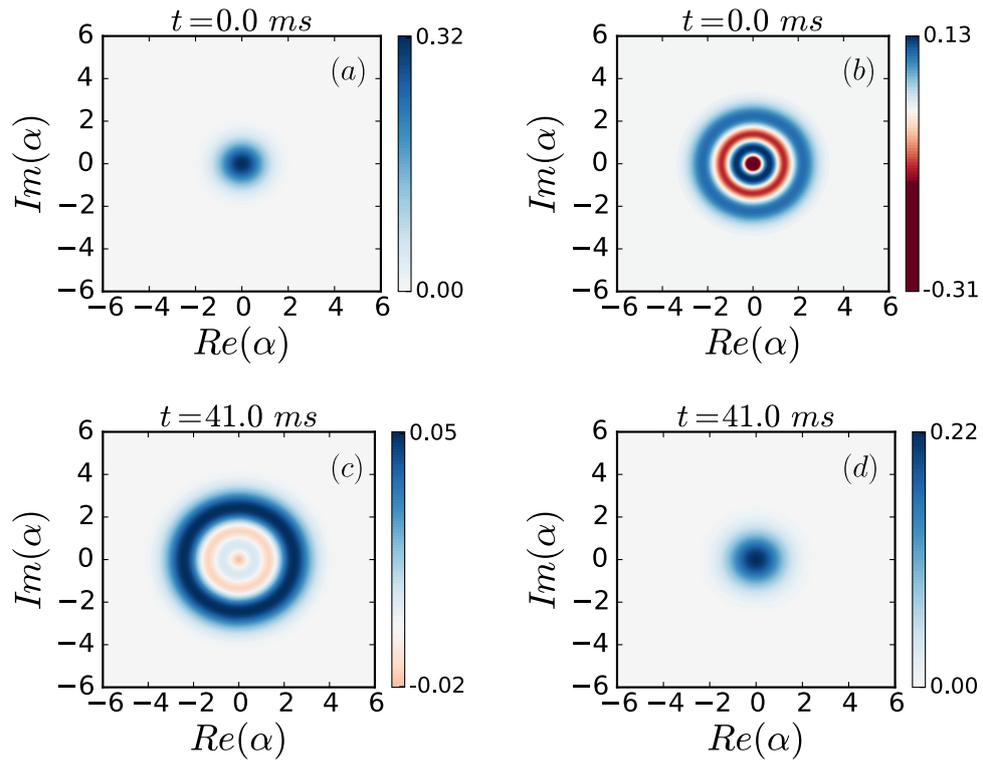
Figure 11. (a), (b): Wigner functions of the initial states of a ground-state cooled ion, i.e. $n = 0$, and a nanowire in the fourth Fock state $n = 3$, respectively. (c), (d): Wigner functions of the swapped states of the ion and the nanowire respectively after 41 ms of interaction at 100 μK bath temperature and 37 Hz coupling strength. The two systems have swapped their initial quantum states at this point in time.

Acknowledgments

References

[1] O'Connell A D et al 2010 Nature **464** 697–703
[2] Teufel J D et al 2011 Nature **475** 359–63
[3] Chan J et al 2011 Nature **478** 89–92
[4] Verhagen E, Deléglise S, Weis S, Schliesser A and Kippenberg T J 2012 Nature **482** 63–7
[5] Nichol J M, Naibert T R, Hemesath E R, Lauchon L J and Budakian R 2013 Phys. Rev. X **3** 031016
[6] Stipe B C, Mamin H J, Stowe T D, Kenny T W and Rugar D 2001 Phys. Rev. Lett. **87** 096801
[7] Rossi N, Braakman F R, Cadeddu D, Vasyukov D, Tütüncüoglu G, Fontcuberta I, Morral A and Poggio M 2017 Nat. Nanotechnol. **12** 150–5
[8] De Lépinay L M, Pigeau B, Besga B, Vincent P, Poncharal P and Arcizet O 2017 Nat. Nanotechnol. **12** 156–62
[9] Aspelmeyer M, Kippenberg T J and Marquardt F 2014 Rev. Mod. Phys. **86** 1391
[10] Pirkkalainen J M, Cho S, Massel F, Tuorila J, Heikkilä T, Hakonen P and Sillanpää M A 2015 Nat. Commun. **6** 6981
[11] Montinaro M, Wüst G, Munsch M, Fontana E, Russo-Averchi E, Heiss M, Fontcuberta I, Morral A, Warburton R J and Poggio M 2014 Nano Lett. **14** 4454
[12] Hunger D, Camerer S, Korppi M, Jöckel A, Hänsch T W and Treutlein P 2011 C. R. Phys. **12** 871–87
[13] Vogell B, Kampschulte T, Rakher M, Faber A, Treutlein P, Hammerer K and Zoller P 2015 New J. Phys. **17** 043044
[14] Chen X, Liu Y C, Peng P, Zhi Y and Xiao Y F 2015 Phys. Rev. A **92** 033841
[15] Stevenson R, Minář J, Hofferberth S and Lesanovsky I 2016 Phys. Rev. A **94** 043813
[16] Tretiakov A and LeBlanc L 2016 Phys. Rev. A **94** 043802
[17] Sanz-Mora A, Eisfeld A, Wüster S and Rost J M 2016 Phys. Rev. A **93** 023816
[18] Hunger D, Camerer S, Hänsch T W, König D, Kotthaus J P, Reichel J and Treutlein P 2010 Phys. Rev. Lett. **104** 143002
[19] Jöckel A, Faber A, Kampschulte T, Korppi M, Rakher M T and Treutlein P 2015 Nat. Nanotechnol. **10** 55–9
[20] Leibfried D, Blatt R, Monroe C and Wineland D J 2003 Rev. Mod. Phys. **75** 281
[21] Ruster T, Schmiegelow C T, Kaufmann H, Warschburger C, Schmidt-Kaler F and Poschinger U G 2016 Appl. Phys. B **122** 254
[22] Schäfer V M, Balance C J, Thirumalai K, Stephenson L J, Ballance T G, Steane A M and Lucas D M 2018 Nature **555** 75
[23] Häffner H, Roos C F and Blatt R 2008 Phys. Rep. **469** 155
[24] Meekhof D M, Monroe C, King B E, Itano W M and Wineland D J 1996 Phys. Rev. Lett. **76** 1796–9

[25] Kienzler D, Lo H Y, Keitch B, De Clercq L, Leupold F, Lindenfelser F, Marinelli M, Negnevitsky V and Home J P 2015 *Science* **347** 53–6
[26] Kienzler D, Flühmann C, Negnevitsky V, Lo H Y, Marinelli M, Nadlinger D and Home J P 2016 *Phys. Rev. Lett.* **116** 140402
[27] Willitsch S 2012 *Int. Rev. Phys. Chem.* **31** 175–99
[28] Germann M, Tong X and Willitsch S 2014 *Nat. Phys.* **10** 820
[29] Chang Y P, Dlugolecki K, Küpper, Rösch D, Wild D and Willitsch S 2013 *Science* **342** 98
[30] Kilaj A, Gao H, Rösch D, Rivero U, Küpper J and Willitsch S 2018 *Nat. Commun.* **9** 2096
[31] Roßnagel J, Dawkins S T, Tolazzi K N, Abah O, Lutz E, Schmidt-Kaler F and Singer K 2016 *Science* **352** 325–9
[32] Tian L and Zoller P 2004 *Phys. Rev. Lett.* **93** 266403
[33] Hensinger W K, Utami D W, Goan H S, Schwab K, Monroe C and Milburn G J 2005 *Phys. Rev.* A **72** 041405
[34] Kotler S, Simmonds R W, Leibfried D and Wineland D J 2017 *Phys. Rev.* A **95** 022327
[35] Singer K, Poschinger U, Murphy M, Ivanov P, Ziesel F, Calarco T and Schmidt-Kaler F 2010 *Rev. Mod. Phys.* **872** 2609
[36] Mokhberi A and Willitsch S 2015 *New J. Phys.* **17** 045008
[37] Blakestad R B, Ospelkaus C, VanDevender A P, Wesenberg J H, Biercuk M J, Leibfried D and Wineland D J 2011 *Phys. Rev.* A **84** 032314
[38] Berkeland D J, Miller J D, Bergquist J C, Itano W M and Wineland D J 1998 *J. Appl. Phys.* **83** 5025
[39] Matthey T, Cickovski T, Hampton S S, Ko A, Ma Q, Nyerges M, Raeder T, Slabach T and Izaguirre J A 2004 *ACM Trans. Math. Softw.* **30** 237
[40] Johansson J, Nation P D and Nori F 2011 *Comput. Phys. Commun.* **183** 1760
[41] Johansson J, Nation P D and Nori F 2013 *Comput. Phys. Commun.* **184** 1234
[42] Lindblad G 1976 *Commun. Math. Phys.* **48** 119
[43] Gerry C G and Knight P L 2005 *Introductory Quantum Optics* (Cambridge: Cambridge University Press)
[44] Alonso J, Leupold F M, Solèr Z U, Fadel M, Marinelli M, Keitch B C, Negnevitsky V and Home J P 2016 *Nat. Commun.* **7** 11243
[45] Home J P, Hanneke D, Jost J D, Leibfried D and Wineland D J 2011 *New J. Phys.* **13** 073026
[46] Kirchmair G, Vlastakis B, Leghtas Z, Nigg S E, Paik H, Ginossar E, Mirrahimi M, Frunzio L, Girvin S M and Schoelkopf R J 2013 *Nature* **495** 205
[47] Laird E, Kuemmeth F, Steele G, Grove-Rasmussen K, Nygård J, Flensberg K and Kouwenhoven L 2015 *Rev. Mod. Phys.* **87** 703
[48] Charlier J, Blase X and Roche S 2007 *Rev. Mod. Phys.* **79** 677
[49] Palma M, Maradan D, Casparis L, Liu T M, Froning F N M and Zumbühl D M 2017 *Rev. Sci. Inst.* **88** 043902